HHS Public Access

Author manuscript

Gene Ther. Author manuscript; available in PMC 2018 February 23.

Published in final edited form as:

Gene Ther. 2017 November ; 24(11): 717–726. doi:10.1038/gt.2017.82.

Stent-based delivery of adeno-associated viral vectors with sustained vascular transduction and iNOS-mediated inhibition of in-stent restenosis

Ilia Fishbein[1,2,*], **David T. Guerrero**[1], **Ivan S. Alferiev**[1,2], **Jonathan B. Foster**[1], **Nicholas G. Minutolo**[1,2], **Michael Chorny**[1,2], **Alejandro Mas Monteys**[1], **Kathryn H. Driesbaugh**[2], **Chandrasekaran Nagaswami**[2], and **Robert J. Levy**[1,2]

[1]The Children's Hospital of Philadelphia

[2]The Perelman School of Medicine of the University of Pennsylvania

Abstract

In-stent restenosis remains an important clinical problem in the era of drug eluting stents. Development of clinical gene therapy protocols for the prevention and treatment of in-stent restenosis is hampered by the lack of adequate local delivery systems. Herein we describe a novel stent-based gene delivery platform capable of providing local arterial gene transfer with adeno-associated viral (AAV) vectors. This system exploits the natural affinity of protein G (PrG) to bind to the Fc region of mammalian IgG, making PrG a universal adaptor for surface immobilization of vector-capturing antibodies (Ab). Our results: 1) demonstrate the feasibility of reversible immobilization of AAV2 vectors using vector tethering by AAV2-specific Ab appended to the stent surface through covalently attached PrG, 2) show sustained release kinetics of PrG/Ab-immobilized AAV2 vector particles into simulated physiological medium *in vitro* and site-specific transduction of cultured cells, 3) provide evidence of long-term (12 weeks) arterial expression of luciferase with PrG/Ab-tethered $AAV2_{Luc}$, and 4) show anti-proliferative activity and anti-restenotic efficacy of stent-immobilized $AAV2_{iNOS}$ in the rat carotid artery model of stent angioplasty.

Introduction

Stent angioplasty, i.e. percutaneous placement of balloon-expandable or self-expandable metallic or polymeric scaffolds in the vascular conduit narrowed by atherosclerotic plaque is a treatment of choice in symptomatic patients with coronary and peripheral atherosclerosis. Approximately 1 million patients in the USA alone undergo this treatment each year [1]. Sophistication of vascular stent designs, especially those which combine mechanical support with local drug delivery, has expanded clinical indications for stent angioplasty resulting in a

*corresponding author Address: 3615 Civic Center Blvd, Philadelphia, PA, 19004, CHOP, ARC, Room 702C, Phone: (215) 590-8740, Fax: (215) 590-5454, fishbein@email.chop.edu.

Conflict of interest

The authors declare no conflict of interest.

decrease of bypass surgery and target lesion revascularization procedures. Nonetheless, even with 3rd generation drug eluting stents (DES), stent failure caused by in-stent restenosis (ISR) remains a significant problem, especially in certain patient populations, such as diabetics [2].

Gene therapy delivered from stent struts directly to the acutely remodeled vessel wall presents an advance compared to DES. The benefits of localized gene therapy implemented in the form of gene delivery stents (GDS) over DES are prolonged modification of the vascular substrate, the selectivity of exerted effects towards smooth muscle cells (SMC) versus endothelium, and a potential combination of the anti-ISR therapy with the interventions preventing progression of atherosclerotic process in the stented artery. Driven by this rationale, attempts have been made to overexpress reporter and therapeutic genes in the stented vasculature of experimental animals using both non-viral [3–5] and viral [6–12] vectors immobilized on stent struts. While generally successful in demonstrating the initial presence of the encoded gene product in the arterial tissue, these studies have typically failed to achieve sustained expression of therapeutic transgenes. Early discontinuation of anti-restenotic treatment was linked to the loss of therapeutic gain at the later time points after the intervention [13]. The studies in the field have identified vector-triggered inflammatory and immune responses resulting in promoter shut-down and vector destruction as the principal causes for the abrogated transgene expression *in vivo* [14, 15]. Additionally, inadequacy of the stent-based delivery system, allowing almost immediate release of the stent-immobilized vector depot, presents a major deficiency in GDS design.

The nature of therapeutic genes capable of inhibiting deleterious remodeling of the stented arteries has been investigated in many studies [16, 17]. We [7, 8] and others [5, 11] have previously demonstrated that augmented nitric oxide production with overexpression of endothelial and inducible isoforms of nitric oxide synthase encoded by gene vectors delivered from the stents inhibits restenosis though multiple mechanisms related to reduced SMC proliferation [18] and migration [19], enhanced endothelial re-growth [20], and decreased ingress of inflammatory cell types into the vascular wall [21]. Our prior work on stent-mediated delivery of inducible nitric oxide synthase (iNOS) for augmenting nitric oxide availability in the stented vasculature employed adenoviral (Ad) vectors [7–9]. Ad_{iNOS} demonstrated anti-restenosis efficacy in the rat carotid model that was optimally enhanced with dietary supplementation of the iNOS substrate, arginine, and its prosthetic co-factor, tetrahydrobiopterin (BH4) [22]. Nevertheless, Ad vectors have multiple shortcomings when developed as human therapeutics [14], and thus are inapplicable for GDS clinical translation beyond the proof of concept phase.

Herein we report on the formulation, characterization and *in vitro* and *in vivo* investigations of a novel stent-based platform for iNOS-encoding adeno-associated viral vector ($AAV2_{iNOS}$) delivery to the stented vasculature. Recently AAV has emerged as the preferred vector in human gene therapy trials due to their low immunogenicity and minimal activation of inflammatory signaling cascades [23]. While AAV of several serotypes were shown to attain transduction of vascular tissue [24–26], only a single study to date has explored the use of AAV in conjunction with stent based delivery [12]. To immobilize transduction-competent AAV particles on the stent struts we re-formulated our previously described chemical

methodology [7, 8] for the bare metal surface functionalization with thiol-reactive, pyridyldithio groups, thus allowing for covalent immobilization of thiolated protein G, a universal affinity binding adaptor for Fc fragment of mammalian IgG. The presence of antibody-binding moiety on the stent surface enables further specific binding of vector-capturing antibodies and subsequent vector tethering. In addition, we identified an optimized monoclonal mouse antibody to intact AAV serotype 2 (AAV2) particles (clone A20) with sufficient affinity to support vector tethering. We then used this antibody to reversibly attach AAV2 vector particles on the PrG-functionalized model surfaces and stainless steel stents to characterize the system in terms of maximal vector capacity, vector release rate, transduction activity *in vitro* and *in vivo*, and therapeutic effects of stent immobilized $AAV2_{iNOS}$ in ISR prevention.

Results

Reversible immobilization of AAV vectors on stainless steel surfaces

A novel vector immobilization strategy illustrated in Fig. 1 was used to reversibly append AAV2 to the surface of stainless steel foil, mesh disk and stent samples. Vector tethering optimization experiments confirmed that IgG attachment to the metal surface is dependent upon the presence of surface immobilized PrG, as evidenced by preferential binding of fluorescently labeled antibody to the PrG-primed surface (Suppl. Fig. 1A) and by depletion of fluorescently labeled IgG from the solution incubated with PrG-treated foil samples, but not with the samples prepared with the omission of PrG (Suppl. Fig. 1B). Additionally, we investigated the effectiveness of vector immobilization as a function of antibody concentration and established the optimal input amounts of the capturing antibody per surface area (Suppl. Fig. 1C).

Formation of an AAV vector monolayer on the surface of stainless steel mesh was confirmed with SEM that showed complete surface coverage with spherical objects of 30–40 nm diameter (Fig. 2B), supposedly representing AAV capsids coated with a 12-nm layer of gold-palladium. Some of these entities appeared to be clustered into groups of 3–5 objects. No such artifacts were observed on the surface of unmodified mesh disks (Fig. 2A).

Release kinetic of PrG-Ab –tethered AAV2 vector *in vitro*

To determine whether antibody tethering of AAV2 particles to the metal surface provides adequate affinity forces to prevent immediate release of immobilized vector, the amount of $AAV2_{iNOS}$ genomes associated with stainless steel foils formulated using the PrG-A20 vector immobilization strategy was determined immediately upon the samples preparation (unreleased samples) and at 7 time points during a 1-month release experiment. Release of vector was carried out at 37°C in simulated medium comprised of 5% human serum albumin/DMEM. Shaking (70 RPM) of the samples was used to simulate the shearing effect of blood flow. Results of the release experiment imply that there are two linear phases of fast (day 0 – day 2) and slow (day 2 – day 31) release of AAV2 particles from the surface of model foils (Suppl. Fig. 2). Approximately 24% of viral load is released during the first 2 days, followed by additional release of 43% of the initial virus load between days 2 and 31.

Overall, two thirds of the viral cargo was dissociated from the metal surface during the first month of *in vitro* release (Suppl. Fig. 2).

In vitro transduction with PrG-Ab –tethered AAV2 vector

To assure that antibody-mediated immobilization of AAV2 vectors does not compromise their transduction capacity, stainless steel mesh disks were formulated with 5×10^8 vector genomes (VG) of $AAV2_{eGFP}$ or 3.5×10^8 VG of $AAV2_{iNOS}$. The samples formulated with omitting the A20 antibody incubation step or both PrG and A20 exposures served as controls in the eGFP expression experiments. The metal disks properly formulated with AAV2-capturing antibody, but lacking exposure with $AAV2_{iNOS}$ were employed as controls in iNOS over-expression studies. Robust eGFP expression was demonstrated 3 days after the placement of PrG/A20-$AAV2_{eGFP}$ meshes in subconfluent HEK cultures, while only minimal transduction was observed in the cell cultures treated with control meshes (Fig 3 A and B). Intensity of eGFP expression in cells transduced with properly immobilized AAV2 vector was further increased by day 12, while no substantial increase of eGFP expression was detected in wells treated with control meshes (Fig. 3 A and B). Notably, the cells transduced with $AAV2_{eGFP}$ eluting meshes were located almost exclusively under the mesh and within 100 μm of mesh disk circumference (Fig. 3A), thus demonstrating site-specificity of gene transfer by Ab-tethered vector.

Inducible nitric oxide synthase activity in HEK293 cells, similarly transduced with mesh-immobilized $AAV2_{iNOS}$ was detected with Griess assay that demonstrated high levels of a stable NO end-product, nitrite, in the media conditioned with mesh-immobilized $AAV2_{iNOS}$, but not in the media from untreated cells or cells treated with PrG/A20-modified mesh samples that were not exposed to $AAV2_{iNOS}$ (Fig. 3C).

Persistence of AAV2 stent load after arterial catheterization and *in vivo* release

To determine physical resilience of the submicronial PABT/PrG/Ab-AAV layer to withstand mechanical impact inherent to vascular catheterization, we quantified with RT-PCR residual AAV2 load in three groups of similarly formulated stents that were surface-modified with $AAV2_{GFP}$: 1) unmanipulated stents; 2) stents inserted via the external carotid arteriotomy site into the mid-segment of the common carotid artery in rat model and immediately retrieved without arterial deployment, and 3) stents deployed in the mid-segment of the common carotid artery and harvested 2 days after implantation. The results of this experiment demonstrate that despite inevitable brushing related to introduction of gene-eluting stents through the unyielding plastic introducer and narrow vascular conduit, approximately 70% of the initial AAV2 load remains associated with the stent (Fig. 4). Moreover, abundant surface AAV2 can still be quantitated after arterial deployment and 2-day release *in vivo* (Fig. 4).

Time course of site-specific arterial expression after implantation of AAV2-Luc –tethered stents in rats

Prior gene delivery stent studies typically reported limited duration of transgene expression in the stented vasculature [3, 4]. To assess kinetics of vascular transduction with our new stent-based AAV2 delivery system, stents formulated with 7.5×10^8 VG of $AAV2_{Luc}$ appended to

the bare stainless steel surface via PABT/PrG/A20 linking system were deployed in the common carotid location in a rat model. The animals then underwent serial bioluminescence imaging at 1, 2, 4 and 12 weeks after stent implantation (Fig. 5A). Localized expression of luciferase spatially corresponding to the location of deployed stent was detected in all animals at all time points (Fig. 5A). Importantly, the signal intensity increased over time reaching a maximum of 4.35×10^6 photons/min/cm^2/steradian at 12 weeks post-stenting (Fig. 5 A and B).

AAV2-iNOS stents attain site-specific transgene expression *in vivo* and enhanced nitric oxide production *ex vivo*

To demonstrate functional competence of locally delivered AAV2 encoding our therapeutic transgene of interest, iNOS, bare metal stents and stents formulated with 4.5×10^8 VG of $AAV2_{iNOS}$ immobilized via PrG/A20 tethering were deployed in the common carotid arteries in a rat model. Ongoing expression of human iNOS in the stented arterial segments explanted 8 days after surgery was determined by RT-PCR and analyzed by the ΔΔCt method, demonstrating baseline expression levels in the arteries treated with BMS. In comparison, a 23-fold higher occurrence of human iNOS transcript was determined in vascular tissue of animals treated with $AAV2_{iNOS}$ eluting stents (Fig. 6A).

In a separate experiment, PrG/A20-modified stents formulated with or without 8×10^8 VG of $AAV2_{iNOS}$ were deployed in the common carotid arteries of rats supplemented with arginine and BH4 via drinking water as previously published [22], to prevent uncoupling of iNOS with the undesirable formation of superoxide and peroxynitrite. Nitric oxide production was determined with Griess assay of the media conditioned by the stented carotid segments harvested at euthanasia (day 8) and cultured *ex vivo* for 72 hours. Compared with arterial tissue from animals treated with PrG/A20-only stents, a 16-fold higher NO production was found in the medium conditioned with $AAV2_{iNOS}$ delivery stents (Fig. 6B).

$AAV2_{iNOS}$ stents inhibit ISR in the rat model of stent angioplasty through mitigation of cell proliferation in stented arteries

To investigate the mechanistic aspects of stent-based delivery of AAV2-$_{iNOS}$ to stent-injured arteries and to validate the therapeutic potential of this intervention, bare metal stents and gene eluting stents (5×10^8 genomic particles of $AAV2_{iNOS}$ immobilized via the PrG/A20 tether) were deployed in two groups of rats supplemented with Arg and BH4. Morphometric analysis of the explanted arteries treated with the stents capable of local arterial delivery of $AAV2_{iNOS}$ gene vector revealed a 31% reduction of the neointimal area (Fig. 7 A and B), without significant changes in the area of the media (Fig. 7 A and C) thus resulting in a 34% decrease of the neointima to media ratio (Fig. 7 A and D). The anti-restenotic effect of $AAV2_{iNOS}$-eluting stents was accompanied by a 47%, 57% and 23% decreases of Ki-67 labeling in the neointima, media and adventitia, respectively, of the GDS-treated compared with BMS-treated arteries (Fig. 8 A and B).

To confirm effective iNOS transduction of $AAV2_{iNOS}$ stent-treated rat arteries, we assessed expression of the DYKDDDDK epitope (FLAG-tag) cloned into human iNOS construct expressed by the AAV vector using immunohistochemistry. This approach allowed us to

avoid ambiguity related to cross-reactivity between endogenous rat iNOS upregulated by vascular intervention [27] and the antibody generated to human iNOS. Massive staining with a cellular pattern was observed in rats treated with AAV-iNOS –eluting stents, while no staining was detected in BMS-treated animals (Suppl. Fig. 3). To elucidate what cell type is predominantly targeted by stent-eluted AAV vectors we used dual immunofluorescence (for FLAG and cell type-specific markers). We found that the vast majority of FLAG-expressing cells are neointimal SMC, although adventitial macrophages are also notably transduced (Suppl. Fig. 4).

Stent-based delivery of $AAV2_{iNOS}$ did not increase stent-triggered inflammation, as inferred from equal prevalence of macrophages in the lesions induced by gene-eluting and control stents (434±81/mm2 and 422±87/mm^2, respectively; Suppl. Fig. 5).

Discussion

The main findings of our study are: 1) demonstration of the feasibility of labile immobilization of AAV vectors on bare metal surfaces through affinity interaction-mediated molecular bridges established between covalently immobilized PrG and the vector-binding antibody; 2) sustained release of AAV2 particles in simulated physiologic medium *in vitro* and localized transduction of cultured cells with AAV2 vector immobilized via PrG/anti-AAV2 antibody tethering; 3) confirmation of reasonable resistance of the AAV2 monolayer established on the surface of a stent to the mechanical abrasion inherent to angioplasty procedure; 4) transduction of the arterial wall with a sustained site-specific expression of encoded transgene by the AAV2 vector eluted from the stent and 5) ISR inhibition in rats treated with $AAV2_{iNOS}$ eluting stents that was at least partially related to the suppression of cell proliferation in the injured vessel wall.

The implementation of human gene therapy protocols for a range of vascular disease, such as atherosclerosis, pulmonary hypertension and restenosis, requires elaboration of clinically acceptable methods for local delivery of gene vectors to the arterial wall, which are yet to be developed. Substrate mediated gene delivery [28], a gene therapy technique based on improved biodistribution and enhanced effectiveness of gene vectors positioned on the interface between the carrying device and the tissue is well suited for cardiovascular applications involving stent implantation. Thick polymeric coatings initially used for bulk immobilization of the vector depot were shown to be highly pro-inflammatory [29] and thus unsuitable in the context of therapeutic GDS. This problem motivated us [7–9, 30] and others [31, 32] to develop techniques for stent immobilization of gene vectors that rely on reversible tethering of vector particles directly to modified metal surfaces of stents thus avoiding the inflammatory reactions triggered by polymeric coatings. Unlike our prior work that used direct attachment of vector-binding moieties to polyallylamine bisphosphonate-modified steel [8], our present studies employed a universal adaptor, PrG that exhibits a strong affinity to the Fc fragments of mammalian IgG [33] and can thus be used as a molecular bridge between the stent surface and vector binding antibody. Engagement of the Fc domain of antibody into affinity pairing with PrG allows for the optimal presentation of antibody molecules with their antigen-binding F(ab) domains opposing the material surface. This arrangement makes the epitope binding sites maximally exposed for vector tethering. Furthermore, due to the system

modularity, it can be readily modified to immobilize a variety of gene vector types, provided that the antibodies to vector capsid or envelopes are available. This versatility of PrG/Ab-based delivery system is exemplified by transduction of primary rat aortic SMC with adenoviral vector immobilized on model meshes with PrG/anti-Ad hexon antibody tether (Suppl. Fig. 6). It is noteworthy that antibodies used for vector immobilization cannot act as neutralizing antibodies, since being themselves immobilized, they dissociate from the vector when the vector is released from the stent (Fig. 1, Step 8).

The number of viral genomes detected in association with the metal samples by two independent assays (PCR and Pico Green assay) is comparable and 10–20 times lower than calculated based on a maximal geometrical capacity of 20–25 nm spherical particles attached to the surface in a monolayer arrangement. This discrepancy is consistent with data [34] reporting that up to 98% of AAV2 preps consist of empty particles devoid of genome. Since antigenically indistinguishable from the DNA-containing counterparts, the empty capsids occupy space on the surface proportional to their prevalence in the prep, but are not registered by viral DNA-based enumeration methods.

Two phase zero-order release kinetics profile of the vector into simulated physiologic medium was demonstrated in our *in vitro* experiments (Suppl. Fig. 2). It is feasible that a fraction of non-specifically bound AAV2 vector held on the surface through the weak hydrophobic forces is responsible for the rapid (burst) release phase (day 0-day 2). When this rapidly mobilizable fraction is exhausted, the further release (day 2-day 31) is mediated solely by the dissociation of the AAV2 from the PrG/A20 tether; a process that is characterized by a slower rate than the initial burst release of the non-specifically bound fraction. Overall, approximately 67% of surface-associated vector genomes are released during the first month, which is comparable to the release of Ad vector appended to a bare metal surface through hydrolysable cross-linkers [7]. While not specifically addressed in the present study, it is feasible to assume that release kinetics can be modulated by the usage of anti-AAV2 antibodies with different affinity (Kd). To that end, dissimilar transduction time course was demonstrated in our prior studies with Ad vectors immobilized through the adapters with different Kd [8]. Moreover, concurrent tethering of several antibody linkers with different Kd on the same stent provides a potential strategy for vector release optimization. Additionally, this modular system is consistent with the simultaneous immobilization of different classes of viral vectors, such as Ad and AAV, or viral and non-viral vectors on the same stent. These intriguing possibilities will be investigated in our future studies.

To study the general aspects of transduction with the metal substrate-immobilized AAV2 vector we used a non-vascular cell type (HEK293) due to its susceptibility to AAV2 transduction (Fig. 3). Remarkably, presence of AAV2-capturing antibody on the surface of mesh disks exposed to $AAV2_{eGFP}$ increased transduction of cells in culture (Fig. 3 A and B), substantiating the proposed immobilization and release paradigm (Fig. 1). The majority of transduced cells were located within 100 microns (3–5 cell diameters) from the mesh borders, consistent with the intended local delivery application of stent-immobilized AAV2 vector. The fluorescence signal emitted by cells transduced with PrG/A20-tethered $AAV2_{eGFP}$ increased 5.5-fold between days 3 and 12. This expression pattern may reflect continuous transduction events mediated by infection-competent AAV2 particles released

from the meshes after the day 3 time point. Similar prolongation of transduction competence upon exposure to the cell culture media at 37°C was demonstrated earlier for Ad vector immobilized on the metal substrate [7].

Mechanical forces inherent to the stent introduction into the vasculature through percutaneous or arteriotomy access, and stent advancement via torturous, narrowed and often calcified vascular conduit to the deployment site present a challenge for the integrity of the vector depot of GDS [35]. Physical dislodgement of the vector en route to the target site decreases the applied vector dose and promotes off-target tissue inoculation. To model vector shearing involved in stent positioning at the target site, groups of similarly formulated $AAV2_{eGFP}$ stents were compared with or without insertion via the introducer tubing and a passage though the common carotid artery, demonstrating that approximately 70% of initial vector dose is still associated with the undeployed stents after their retrieval from the vasculature (Fig. 4). This is an expected result since the vector depot is not coated with any protective polymer layer to avoid additional inflammatory stimuli. We did not investigate the fate of the dislodged $AAV2_{eGFP}$ in these experiments. Based on published reports, most of the systemically administered vector ends up in liver [36]. The dose of the vector released into circulation (ca 2.2×10^8 VG) is at least 1000-fold lower than a tolerated dose in published systemic AAV administration studies [37] and is not expected to cause toxicity and systemic inflammation. Nonetheless, our future studies will explore a possibility of AAV2 depot stabilization using chemical cross-linking of surface-bound AAV2.

Approximately 75% of the dose that was associated with the stents at the time of deployment was found to be released during the first 48 hours. Faster vector release *in vivo* (Fig. 4) compared to the cell-free *in vitro* system (Suppl. Fig. 2) might be attributed to more aggressive release medium, decreased pH of tissue fluid due to acute inflammation at the site of stent deployment, the shearing effect of blood flow, and vector interaction with vascular and blood-borne cells. Overall, in situ release of the vector is more sustained than reported for non-viral [3, 38] and Ad [10] vectors. Since restenotic neointima is not present at the time of stent implantation, the capability of GDS to sustain release of the transduction-competent vector is crucial if neointimal SMC are considered as the target cell type for GDS intervention.

AAV is currently the most promising vector for human gene therapy, due to its satisfactory safety profile, minimal instigation of inflammatory and immunological reactions and long-term expression in the host [23, 39]. Currently, only a single study has investigated a time course of vascular transduction with stent immobilized AAV2 vectors [12], finding a 2.7-fold drop in the number of βGal-transduced cells from 3 to 28 days post-stenting. Contrary to these results, our longitudinal bioluminescence studies in rats treated with $AAV2_{Luc}$-configured stents (Fig. 5), demonstrated escalating luciferase expression (day 7 to day 84). A luminescence signal co-localized with stent location in all cases. The potential reasons for the discrepancy between our data and those of Sharif et al [12] may be 1) delivery system (PrG/A20 mediated tethering of AAV2 vs. AAV2 entrapment in a phosphorylcholine coating on a surface of BiodivYsio stent); 2) animal model (rat carotid vs. rabbit iliac stent implantation) and 3) a high immunogenicity of βGal [40] resulting in mounting substantial immune response toward βGal-expressing cells.

Interventions aimed at restoring the nitric oxide balance in balloon injured and stented arteries have demonstrated the therapeutic potential for alleviating restenosis through multiple synergistic mechanisms related to inhibition of platelet aggregation [41], SMC proliferation [18] and migration [19], curtailing inflammatory reactions [21] and promoting re-endothelialization [20]. In our previous studies Ad_{iNOS} in the stent-immobilized form and as a free vector was shown to inhibit restenosis in the rat model[7, 8, 22]. To validate both transduction of arterial tissue with $AAV2_{iNOS}$ vector and the anticipated physiological effects of iNOS overproduction, we constructed AAV2 vectors with human iNOS sequence to be able to distinguish a vector-overexpressed transgene from the endogenous rat iNOS, which was shown to be actuated by vascular injury [27]. Super-physiological levels of iNOS production in the vascular tissue can result in relative deficiency of Arg and BH4 with ensuing iNOS decoupling which leads to production of damaging reactive oxygen species [42]. To prevent this, animals in our $AAV2_{iNOS}$ stent studies were supplemented with Arg and BH4 through the drinking water. Human iNOS-specific primers were able to support amplification of DNA sequence that was reverse-transcribed using RNA extracted from the carotid arteries treated by $AAV2_{iNOS}$ GDS, but not by BMS (Fig. 6A). Moreover, the over-expressed human iNOS was translated in a protein that maintained functionality in rat vasculature, as evidenced by highly elevated NO production in the media conditioned with $AAV2_{iNOS}$ GDS-transduced arteries compared to the media conditioned with stents that were similarly formulated aside from the vector acquisition (Fig. 6B). The optimal levels of NO production for the prevention of restenosis in balloon injured or stented arteries remains largely unknown. In a similar *ex vivo* assay [43] nitrite accumulation in the media conditioned by the rat carotid arteries transduced with free Ad-iNOS (2×10^6 pfu) was an order of magnitude lower than in our experiments, which is reasonable, considering much lower vector titer and a limited contact time of the vector with the vessel wall.

A 34% inhibition of ISR was observed in our therapeutic study in Arg/BH4-supplemented animals treated with the $AAV2_{iNOS}$ GDS compared to BMS-treated counterparts (Fig. 7). Our previously published experiments with Ad_{iNOS}-eluting stents formulated with Coxsackie-Adenovirus receptor D1 domain-mediated affinity binding of the vector [8] or with covalent vector attachment via hydrolysable cross-linkers [7] demonstrated a ~50% reduction of ISR. Moreover, in a model of indwelling delivery of free Ad_{iNOS} suspension to Fogarty balloon injured rat arteries a subtotal 95% inhibition of restenosis was observed [44], supporting the role of nitric oxide as a principal anti-restenotic mediator.

Neointimal formation triggered by stent implantation in healthy rat arteries is limited and typically results in a 20–25% luminal narrowing with a 30–80 μm layer of neointimal tissue over the struts. While stent-based delivery of Ad_{iNOS} achieved a stronger neointimal inhibition than was observed in our present study with $AAV2_{iNOS}$-eluting stents, it was associated with a high percentage of uncovered struts, which in humans is a proven risk factor of stent thrombosis [45]. The extent of ISR is much greater in human atherosclerotic arteries, where subtotal (>90%) occlusions of the stented segment with neointimal tissue is a common finding [46]. Since nitric oxide is deficient in atherosclerotic arteries [47], it is feasible that in the atherosclerotic milieu, stents designed to deliver gene therapy for nitric oxide augmentation will show a larger therapeutic gain than in healthy rats. To this end, the ultimate clinical translatability of $AAV2_{iNOS}$ GDS should be investigated in a diseased

animal model, such as the atherosclerotic rabbit iliac artery [48] or the coronary artery of diabetic hypercholesterolemic swine [49].

Some limitations of our studies should be mentioned. The antirestenotic effects of a single fixed dose of AAV-iNOS were investigated *in vivo*. It is possible that the therapeutic effects can be enhanced with the adjustment of the vector dose. The impact of stent-based delivery of $AAV2_{iNOS}$ on recovery of denuded endothelium in the stented artery was not determined, and this should be the subject of advanced investigations. Off-target transduction of perivascular tissue and distant organs was also not studied. The rat carotid model used in these experiments, involving healthy animals, is known to be more permissive in terms of therapeutic effectiveness than more stringent human-like porcine models involving hypercholesterolemia and diabetes.

In conclusion, the present studies demonstrate immobilization of viable AAV2 vectors on bare metal surfaces through the affinity bridges consisting of PrG and an AAV2-specific antibody. The amount of a surface-immobilized vector is consistent with a monolayer arrangement of the vector particles on the surface. Antibody-mediated binding bestows sustained release properties to immobilized vector and provides site-specific transduction *in vitro* and *in vivo*. In the rat carotid model, stents formulated with surface-bound AAV2 demonstrate escalating expression of encoded transgene (luciferase) for 12 weeks and ISR mitigation with overexpression of inducible nitric oxide synthase.

Materials and Methods

Materials

Stainless steel (grade 316) foil sheets were purchased from Goodfellow (Coraopolis, PA). Stainless steel (grade 316) mesh disks (3 mm diameter) were purchased from Electron Microscopy Sciences (Hatfield, PA). Multilink stainless steel (grade 304) stents were custom made by Laserage (Waukegan, IL). The angioplasty catheters were donated by NuMED (Hopkinton, NY). Polyallylamine bisphosphonate with latent thiol groups (PABT) and pyridyldithio-engrafted polyethyleneimine (PEI-PDT) were synthesized in-house according to previously published [7] methods. Tris (2-carboxyethyl) phosphine hydrochloride (TCEP·HCl) was obtained from Thermo Fisher Scientific (Waltham, MA). The thiolated form of protein G (PrG-SH) was purchased from Protein Mods (Madison, WI). Anti-AAV2 (clone A20), anti-Ad hexon and anti-Ki67 antibodies were obtained from GeneTex (Irvine, CA), Biodesign International (Saco, ME) and Novus Biologicals (Littleton, CO), respectively. All other chemicals and solvents were purchased from Sigma-Aldrich (St. Louis, MO) and VWR International (Radnor, PA).

All reporter gene vectors used in the present studies ($AAV2_{eGFP}$, $AAV2_{Luc}$, and Ad_{eGFP}) were constructed and produced in the Vector Core facility of the University of Pennsylvania. $AAV2_{iNOS}$ was produced by the Research Vector Core at the Center for Cellular and Molecular Therapeutics of the Children's Hospital of Philadelphia (CHOP).

Vector immobilization protocol (Fig. 1)

Stainless steel stents, mesh disks and foils coupons were cleaned with isopropanol and incubated in a 0.5% aqueous solution of polyallylamine bisphosphonate with latent thiol groups (PABT; [7]) at 60°C with shaking for 1 hour (Fig.1, Step 1). Acidity of the solution was adjusted with potassium bicarbonate to pH of 4.5. After washing the samples in double distilled water (DDW), thiol groups in the side chains of PABT were deprotected with tris (2-carboxyethyl) phosphine hydrochloride (TCEP·HCl; 10 mg/ml in 0.1M acetate buffer, pH 4.5; at room temperature (RT) with shaking for 15 min; Fig.1, Step 2). The samples were then thoroughly washed with degassed DDW and reacted with an 0.5% aqueous solution of pyridyldithio-engrafted polyethyleneimine (PEI-PDT; [7]) at 28°C with shaking for 1 hour (Fig. 1, Step 3) followed by the incubation with thiolated protein G (PrG-SH; 125 μg/ml in degassed PBS; at 28°C with shaking for 1 hour; Fig. 1, Step 4). After extensive washing of the samples, an antibody of required specificity, e.g. anti-AAV2 (clone A20), diluted in PBS to the volume sufficient to completely cover the samples and providing 2–5 μg of antibody/cm^2 of metal surface was added to the samples at 28°C with mild shaking for 45 min (Fig. 1, Step 5). The samples were washed in PBS and incubated with AAV2 suspension (10^{10} VG/ml PBS) at 28°C with mild shaking for 45 min (Fig. 1, Step 6), resulting in capturing of AAV2 particles on the surface of metal samples (Fig. 1, Step 7) thus enabling subsequent release of the vector *in vitro* and *in vivo* (Fig. 1, Step 8).

Quantification of the vector load associated with metal surface

To determine the number of AAV2 genomic particles on the surface of metal samples two methods were employed.

qPCR of vector transgene sequence—The vector genome (VG) number of $AAV2_{eGFP}$ attached to the metal surface was determined by qPCR as reported by us before [9, 30]. In brief, AAV2 was eluted from the surface and lysed using 2-hour incubation at 56°C in proteinase K diluted in ALT buffer. Viral DNA was extracted and purified using QIAamp DNA Mini kit per manufacturer instructions. Transgene sequence was amplified in a Sybr Green-registered reaction using eGFP-specific primers (forward: 5’ CTC CTC GCC CTT GCT CAC 3’, reverse: 5’ CAG TGG ATG TTG CCT TTA CTT CTA G 3’). Serial dilutions of free $AAV2_{eGFP}$ of a known titer were similarly processed through the isolation and qPCR protocols to generate a calibration curve.

Fluorimetric detection of AAV2 DNA with Pico Green assay—Alternatively, AAV2 VG number was determined with Pico Green assay as recently reported [50] with minor modifications. In brief, AAV2 particles immobilized on metal substrate were lysed in a buffer comprising 10 mM Tris·HCl, 100 mM NaCl and 0.1% SDS at 70°C for 1 hour, followed by a rapid cooling of lysate to 25°C (5°/min) to anneal single stranded DNA fragments. 20-μl aliquots of AAV2 lysates were added into individual wells of a 96-well fluorimetry plate prefilled with 180 μl of Pico Green diluted 1:160 in Tris-EDTA buffer. Fluorescence was measured at 485/538 nm within 5 min of components mixing (Gemini EM, Molecular Devices, Sunnyvale, CA). A calibration curve was constructed using the dilution series prepared from a free AAV2 of a known titer that were similarly processed.

Scanning electron microscopy (SEM)

$AAV2_{eGFP}$ was immobilized on the stainless steel mesh disks via the PrG-A20 tethering at the density of 5×10^8 VG/mesh (per qPCR). Unmodified meshes were used as control. Immediately upon preparation the meshes were rinsed in cacodylate buffer, and fixed in 2% glutaraldehyde/cacodylate buffer followed by alcohol dehydration, HMDS drying and sputter-coating with gold palladium. The surface of meshes was then imaged at 80,000 magnification using a Quanta FEG 250 system (FEI, Hillsboro, OR) to visualize individual AAV2 particles on the metal surface.

Cell transduction experiments

Stainless steel mesh disks were modified with PABT, PEI-PDT, PrG and anti-AAV2 antibody as delineated in the Vector Immobilization Protocol section, prior to the exposure of the samples to 10^{10} VG of $AAV2_{eGFP}$. The resulting mesh vector loading amounted to 5×10^8 VG of $AAV2_{eGFP}$, as determined by qPCR. Control meshes were formulated omitting the PrG and/or capturing antibody attachment steps and were exposed to the same vector suspension as the properly formulated samples. Following PBS washing, the meshes were individually placed in the wells of 96-well plates with subconfluent cultures of HEK 293 cells. Transduction was assessed 3 and 12 days after mesh placement by fluorescence microscopy and fluorimetry.

In a separate study, meshes configured with 3.5×10^8 VG of $AAV2_{iNOS}$ immobilized via PrG/A20 tether were placed into subconfluent HEK 293 cell cultures. Control samples were similarly modified with PrG and A20, but were not exposed to $AAV2_{iNOS}$. iNOS activity in transduced cells was determined with Griess assay [7] by quantifying levels of the stable nitric oxide end-product, nitrites, in the conditioned media.

Engineering of a shuttle plasmid for production of AAV2-iNOS

The human iNOS cDNA sequence was moved into an AAV shuttle vector using standard molecular biology techniques. Human iNOS cDNA sequence containing both a Myc and a DYKDDDDK tag (FLAG) epitope was expressed under the control of the CMV promoter sequence and cloned upstream of the BgH poly A sequence. The human iNOS expression cassette was flanked at each end by AAV serotype 2 145-bp inverted repeat sequences. AAV2 vectors were generated by triple transfection technique in the Research Vector Core at the Center for Cellular and Molecular Therapeutics (CHOP).

Rat carotid model of stent angioplasty

All animal procedures employed in the reported studies conform to federal regulations on laboratory consequently animal use and were preapproved by the Institutional Animal Care and Use Committee of CHOP. All rats were obtained from the same supplier and were used consecutively. No special randomization beyond successive use of animals was performed. The pre-established exclusion criteria in our animal studies were a significant deviation from the standard surgical protocol; morbidity beyond day 2 post-surgery, and thrombosis of the stented vessel. Male Sprague-Dawley rats (10–11 weeks of age; 375–425 gram) were pre-treated with aspirin (3 mg/kg via drinking water for 2 days prior the intervention) and were administered heparin 200 U/kg via the tail vein. Under ketamine (80 mg/kg) and xylazine (5

mg/kg) anesthesia, the skin and fascia of the neck region were dissected to access the bifurcation of the left carotid artery. A 2-F Fogarty catheter was introduced into the common carotid artery through a 2-mm arteriotomy site in the left external carotid artery. The endothelial layer of the common carotid artery was then abrased by three passages of the inflated balloon on the tip of the catheter. Teflon introducer tubing was then placed in the external carotid artery over the Fogarty catheter and the Fogarty catheter was removed. A stent-loaded angioplasty catheter (10 mm length, 1.5 mm nominal diameter; NuMED, Hopkinton, NY) was inserted through the introducer into carotid circulation, advanced to the mid-segment of the carotid arteries, and deployed at 14 atm. The operator was not blinded to the group allocation. After retrieving the angioplasty catheter, the external carotid artery was tied-off, the fascia and skin were repaired, and the animals were recovered.

Vector dislodgment en route to the deployment site and *in vivo* release

Twelve stents were formulated with PrG/A20 tethers and incubated with 10^{10} VG of $AAV2_{eGFP}$ as specified in the Vector Immobilization Protocol section. One group of $AAV2_{eGFP}$ loaded stents (n=4) was mock-deployed on the bench and the expanded stents were removed from the catheters and stored at −20°C pending viral DNA isolation and PCR. A second group of stents (n=4) was inserted via an introducer into the external carotid arteries of rats and advanced to the mid-segment of the common carotid arteries. The stents were then withdrawn from the carotid artery without deployment. Immediately after withdrawal, these stents were expanded, removed from the catheters and stored at −20°C. A third group of stents (n=4) was inserted through the introducer, advanced into the mid-segment of the common carotid artery and deployed *in vivo*. The stented arteries were harvested 2 days post-stenting and the stents were carefully separated from the arterial tissue using a dissecting microscope. Viral DNA was isolated from all stent samples with a QIAamp DNA mini-kit and amplified with RT-PCR using GFP-specific primers.

Bioluminescence imaging

Stents were formulated with 7.5×10^8 VG of $AAV2_{Luc}$ immobilized on the stent surface with PrG/A20 tethering. Stents were then deployed in the Fogarty balloon-injured common carotid arteries of the male Sprague-Dawley rats (n=4). One, two, four and twelve weeks after stent implantation, the animals were anesthetized with isoflurane and their operative wounds were re-opened. Fifty mg of D-luciferin potassium salt (Gold Biotechnology, St. Louis, MO) dissolved in 1 ml PBS was injected through the tail vein. Within 1 min of luciferin administration, the animal was placed in the supine position in a bioluminescence imager (IVIS Spectrum) and the overlay image (photograph and bioluminescence) of the neck and upper chest region was acquired. The skin and fascia were repaired and the animal was recovered and re-imaged at a later time point.

Arterial expression of transgene following $AAV2_{iNOS}$ stent implantation

Arterial segments treated with BMS (n=4) and $AAV2_{iNOS}$-eluting stents configured with 4.5×10^8 VG of $AAV2_{iNOS}$ immobilized on the stent surface via PrG/A20 tethering (n=4) were harvested at the animals' sacrifice (day 8 post-stenting) and homogenized under liquid nitrogen in an ALT lysis buffer. RNA was extracted from the lysed arterial tissue using a RNeasy fibrous tissue mini kit (Qiagen, Germantown, MD), reverse transcribed using a

Taqman Reverse Transcription kit (Applied Biosystems, Foster City, CA), and the cDNA was amplified using human iNOS sequence-specific primers (forward: 5' TTTCCTTACGAGGCGAAGAAG 3', reverse: 5' ATCATTTGCTGCCAGATCCT 3'). To assure the specificity of the primer set to human versus endogenous rat iNOS sequence, the reverse primer was chosen to bind in the Myc-DDK tag portion of the transgene.

Quantification of nitric oxide production by the stented arteries *ex vivo*

Rats were maintained on medicated water providing supplementation of arginine (250 mg/kg/day) and BH4 (10 mg/kg/day) for 2 days prior to stent implantation and until sacrifice using a previously optimized protocol [22]. The animals were treated with gene delivery stents formulated with 8×10^8 VG of $AAV2_{iNOS}$ appended through PrG/A20 tethering (n=4) and with PrG/A20 stents that were not loaded with the gene vector (n=4). The animals were euthanized 8 days post-surgery. The harvested stented arterial segments were intraluminally flushed with sterile saline and placed into individual wells of a 24-well plate prefilled with F12/DMEM medium supplemented with 10% FBS and antibiotics. Non-manipulated left and right carotid arteries from 2 donor rats harvested at the same time as the stented arteries were also cultured *ex vivo* as the additional controls. Griess assays [7] were performed on the media conditioned with the individual arteries 3 days after establishing *ex vivo* cultures.

Morphometric studies

BMS (n=10) and gene eluting stents (8×10^8 VG of AAV immobilized via the PrG/A20 tether; n=10) were deployed in the Fogarty balloon injured carotid arteries of male Sprague-Dawley rats treated with arginine (250 mg/kg/d) and BH4 (10 mg/kg/d) for the duration of the experiment, starting at day 2 before the intervention. The animals were sacrificed 2 weeks post-stenting. The stented carotid segments were harvested, fixed in 10% neutral formalin and acid-treated to dissolve stent struts [51] prior to routine paraffin embedding and sectioning. Verhoeff-van Gieson stained sections were photomicrographed at 40x. The extent of restenosis, expressed as the neointima to media areas ratio, was derived from the morphometric measurements performed using Image J software. The investigator performing morphometry was blinded to the group allocation of histological samples.

Ki-67 immunohistochemistry

A subset of slides from the animals treated with BMS (n=4) and $AAV2_{iNOS}$ eluting stents (n=4) were immunostained with anti-Ki67 antibody (1:100) to determine the prevalence of proliferating cells in the neointima, media and adventitia of the stented arterial segments. A secondary horse anti-rabbit biotinylated antibody (Vector labs, BA-1100), Vectostain ABC Elite peroxidase kit (Vector labs, PK-6100) and 3, 3' diaminobenzidine chromogen (Vector labs, SK-4105) were used as recommended by the manufacturer for color development. The slides were counterstained with Gill-3 hematoxylin, mounted and photographed at 200x. The number of Ki-67 –positive cells in individual arterial compartments was determined for each image (Image J) by counting cell nuclei after converting the image into a black and white 16-bit image and adjusting threshold to visually match the original image. The number of proliferating cells was then normalized by the area of the respective arterial compartment in the captured image, and averaged over 4 images obtained for each slide.

Statistics

In all studies (in vitro and in vivo) the sample size was chosen empirically based on prior experience with identical or closely related models and experimental settings. Data are presented as means ± standard deviation, unless specified otherwise. Gaussian distribution of values within the experimental groups was tested using the Kolmogorov-Smirnov method. Statistical analysis of the difference between groups was performed using analysis of variance (ANOVA), followed by Tukey's test. Statistical significance was noted where $p \leq 0.05$.

Supplementary Material

Refer to Web version on PubMed Central for supplementary material.

Acknowledgments

This work was supported in part by research grants from the National Heart, Lung and Blood Institute including R56-HL 72108, R01HL137762, R01-HL111118, R21- HL131016. Support was also provided by the William J. Rashkind Endowment and Erin's Fund of the Children's Hospital of Philadelphia. PTA catheters were kindly provided by NuMed (Hopkinton, NY). Authors wish to acknowledge Ms. Susan Kerns for preparing the manuscript materials for publication.

References

1. Mozaffarian D, Benjamin EJ, Go AS, Arnett DK, Blaha MJ, Cushman M, et al. Heart Disease and Stroke Statistics-2016 Update: A Report From the American Heart Association. Circulation. 2016; 133(4):e38–360. [PubMed: 26673558]
2. Roffi M, Angiolillo DJ, Kappetein AP. Current concepts on coronary revascularization in diabetic patients. Eur Heart J. 2011; 32(22):2748–57. [PubMed: 21893486]
3. Brito LA, Chandrasekhar S, Little SR, Amiji MM. In vitro and in vivo studies of local arterial gene delivery and transfection using lipopolyplexes-embedded stents. J Biomed Mater Res A. 2010; 93(1):325–36. [PubMed: 19569206]
4. Ganly S, Hynes SO, Sharif F, Aied A, Barron V, McCullagh K, et al. Liposomal surface coatings of metal stents for efficient non-viral gene delivery to the injured vasculature. J Control Release. 2013; 167(2):109–19. [PubMed: 23403396]
5. Sharif F, Hynes SO, McCullagh KJ, Ganley S, Greiser U, McHugh P, et al. Gene-eluting stents: non-viral, liposome-based gene delivery of eNOS to the blood vessel wall in vivo results in enhanced endothelialization but does not reduce restenosis in a hypercholesterolemic model. Gene Ther. 2012; 19(3):321–8. [PubMed: 21716298]
6. Appleby CE, Ranjzad P, Williams PD, Kakar SJ, Driessen A, Tijsma E, et al. Periluminal expression of a secreted transforming growth factor-beta type II receptor inhibits in-stent neointima formation following adenovirus-mediated stent-based intracoronary gene transfer. Hum Gene Ther. 2014; 25(5):443–51. [PubMed: 24483849]
7. Fishbein I, Alferiev I, Bakay M, Stachelek SJ, Sobolewski P, Lai M, et al. Local delivery of gene vectors from bare-metal stents by use of a biodegradable synthetic complex inhibits in-stent restenosis in rat carotid arteries. Circulation. 2008; 117(16):2096–103. [PubMed: 18413497]
8. Fishbein I, Alferiev IS, Nyanguile O, Gaster R, Vohs JM, Wong GS, et al. Bisphosphonate-mediated gene vector delivery from the metal surfaces of stents. Proc Natl Acad Sci USA. 2006; 103(1):159–64. [PubMed: 16371477]
9. Fishbein I, Forbes SP, Chorny M, Connolly JM, Adamo RF, Corrales RA, et al. Adenoviral vector tethering to metal surfaces via hydrolyzable cross-linkers for the modulation of vector release and transduction. Biomaterials. 2013; 34(28):6938–48. [PubMed: 23777912]

10. Johnson TW, Wu YX, Herdeg C, Baumbach A, Newby AC, Karsch KR, et al. Stent-based delivery of tissue inhibitor of metalloproteinase-3 adenovirus inhibits neointimal formation in porcine coronary arteries. Arterioscler Thromb Vasc Biol. 2005; 25(4):754–9. [PubMed: 15681295]
11. Sharif F, Hynes SO, Cooney R, Howard L, McMahon J, Daly K, et al. Gene-eluting stents: adenovirus-mediated delivery of eNOS to the blood vessel wall accelerates re-endothelialization and inhibits restenosis. Mol Ther. 2008; 16(10):1674–80. [PubMed: 18714308]
12. Sharif F, Hynes SO, McMahon J, Cooney R, Conroy S, Dockery P, et al. Gene-eluting stents: comparison of adenoviral and adeno- associated viral gene delivery to the blood vessel wall in vivo. Human gene therapy. 2006; 17(7):741–50. [PubMed: 16839273]
13. Carter AJ, Aggarwal M, Kopia GA, Tio F, Tsao PS, Kolata R, et al. Long-term effects of polymer-based, slow-release, sirolimus-eluting stents in a porcine coronary model. Cardiovasc Res. 2004; 63(4):617–24. [PubMed: 15306217]
14. Hendrickx R, Stichling N, Koelen J, Kuryk L, Lipiec A, Greber UF. Innate immunity to adenovirus. Hum Gene Ther. 2014; 25(4):265–84. [PubMed: 24512150]
15. Qin L, Ding Y, Pahud DR, Chang E, Imperiale MJ, Bromberg JS. Promoter attenuation in gene therapy: interferon-gamma and tumor necrosis factor-alpha inhibit transgene expression. Hum Gene Ther. 1997; 8(17):2019–29. [PubMed: 9414251]
16. Appleby CE, Kingston PA. Gene therapy for restenosis--what now, what next? Curr Gene Ther. 2004; 4(2):153–82. [PubMed: 15180583]
17. Fishbein I, Chorny M, Adamo RF, Forbes SP, Corrales RA, Alferiev IS, et al. Endovascular Gene Delivery from a Stent Platform: Gene- Eluting Stents. Angiol Open Access. 2013; 1(2)
18. Groves PH, Banning AP, Penny WJ, Newby AC, Cheadle HA, Lewis MJ. The effects of exogenous nitric oxide on smooth muscle cell proliferation following porcine carotid angioplasty. Cardiovasc Res. 1995; 30(1):87–96. [PubMed: 7553728]
19. Sarkar R, Meinberg EG, Stanley JC, Gordon D, Webb RC. Nitric oxide reversibly inhibits the migration of cultured vascular smooth muscle cells. Circ Res. 1996; 78(2):225–30. [PubMed: 8575065]
20. Papapetropoulos A, Garcia-Cardena G, Madri JA, Sessa WC. Nitric oxide production contributes to the angiogenic properties of vascular endothelial growth factor in human endothelial cells. J Clin Invest. 1997; 100(12):3131–9. [PubMed: 9399960]
21. De Caterina R, Libby P, Peng HB, Thannickal VJ, Rajavashisth TB, Gimbrone MA Jr, et al. Nitric oxide decreases cytokine-induced endothelial activation. Nitric oxide selectively reduces endothelial expression of adhesion molecules and proinflammatory cytokines. J Clin Invest. 1995; 96(1):60–8. [PubMed: 7542286]
22. Forbes SP, Alferiev IS, Chorny M, Adamo RF, Levy RJ, Fishbein I. Modulation of NO and ROS production by AdiNOS transduced vascular cells through supplementation with L-Arg and BH4: implications for gene therapy of restenosis. Atherosclerosis. 2013; 230(1):23–32. [PubMed: 23958248]
23. Zaiss AK, Muruve DA. Immune responses to adeno-associated virus vectors. Curr Gene Ther. 2005; 5(3):323–331. [PubMed: 15975009]
24. Gruchala M, Bhardwaj S, Pajusola K, Roy H, Rissanen TT, Kokina I, et al. Gene transfer into rabbit arteries with adeno-associated virus and adenovirus vectors. J Gene Med. 2004; 6(5):545–54. [PubMed: 15133765]
25. Lompre AM, Hadri L, Merlet E, Keuylian Z, Mougenot N, Karakikes I, et al. Efficient transduction of vascular smooth muscle cells with a translational AAV2.5 vector: a new perspective for in-stent restenosis gene therapy. Gene Ther. 2013; 20(9):901–12. [PubMed: 23535897]
26. Pankajakshan D, Makinde TO, Gaurav R, Del Core M, Hatzoudis G, Pipinos I, et al. Successful transfection of genes using AAV-2/9 vector in swine coronary and peripheral arteries. J Surg Res. 2012; 175(1):169–75. [PubMed: 21529824]
27. Hansson GK, Geng YJ, Holm J, Hardhammar P, Wennmalm A, Jennische E. Arterial smooth muscle cells express nitric oxide synthase in response to endothelial injury. J Exp Med. 1994; 180(2):733–8. [PubMed: 7519246]
28. Bengali Z, Shea LD. Gene Delivery by Immobilization to Cell-Adhesive Substrates. MRS Bull. 2005; 30(9):659–662. [PubMed: 19319206]

29. van der Giessen WJ, Lincoff AM, Schwartz RS, van Beusekom HM, Serruys PW, Holmes DR Jr, et al. Marked inflammatory sequelae to implantation of biodegradable and nonbiodegradable polymers in porcine coronary arteries. Circulation. 1996; 94(7):1690–7. [PubMed: 8840862]
30. Fishbein I, Forbes SP, Adamo RF, Chorny M, Levy RJ, Alferiev IS. Vascular gene transfer from metallic stent surfaces using adenoviral vectors tethered through hydrolysable cross-linkers. J Vis Exp. 2014; (90):e51653. [PubMed: 25145470]
31. Chang H, Ren KF, Zhang H, Wang JL, Wang BL, Ji J. The (PrS/HGF-pDNA) multilayer films for gene-eluting stent coating: Gene-protecting, anticoagulation, antibacterial properties, and in vivo antirestenosis evaluation. J Biomed Mater Res B, Appl Biomater. 2015; 103(2):430–9. [PubMed: 24909849]
32. Jewell CM, Zhang J, Fredin NJ, Wolff MR, Hacker TA, Lynn DM. Release of plasmid DNA from intravascular stents coated with ultrathin multilayered polyelectrolyte films. Biomacromolecules. 2006; 7(9):2483–91. [PubMed: 16961308]
33. Akerstrom B, Bjorck L. A physicochemical study of protein G, a molecule with unique immunoglobulin G-binding properties. J Biol Chem. 1986; 261(22):10240–7. [PubMed: 3733709]
34. Sommer JM, Smith PH, Parthasarathy S, Isaacs J, Vijay S, Kieran J, et al. Quantification of adeno-associated virus particles and empty capsids by optical density measurement. Mol Ther. 2003; 7(1):122–8. [PubMed: 12573625]
35. Tan A, Farhatnia Y, de Mel A, Rajadas J, Alavijeh MS, Seifalian AM. Inception to actualization: next generation coronary stent coatings incorporating nanotechnology. J Biotechnol. 2013; 164(1): 151–70. [PubMed: 23376617]
36. Paneda A, Vanrell L, Mauleon I, Crettaz JS, Berraondo P, Timmermans EJ, et al. Effect of adeno-associated virus serotype and genomic structure on liver transduction and biodistribution in mice of both genders. Hum Gene Ther. 2009; 20(8):908–17. [PubMed: 19419275]
37. Ferreira V, Twisk J, Kwikkers K, Aronica E, Brisson D, Methot J, et al. Immune responses to intramuscular administration of alipogene tiparvovec (AAV1-LPL(S447X)) in a phase II clinical trial of lipoprotein lipase deficiency gene therapy. Hum Gene Ther. 2014; 25(3):180–8. [PubMed: 24299335]
38. Ohtani K, Egashira K, Nakano K, Zhao G, Funakoshi K, Ihara Y, et al. Stent-based local delivery of nuclear factor-kappaB decoy attenuates in-stent restenosis in hypercholesterolemic rabbits. Circulation. 2006; 114(25):2773–9. [PubMed: 17130346]
39. Nathwani AC, Tuddenham EG, Rangarajan S, Rosales C, McIntosh J, Linch DC, et al. Adenovirus-associated virus vector-mediated gene transfer in hemophilia B. N Engl J Med. 2011; 365(25): 2357–65. [PubMed: 22149959]
40. Tsujinoue H, Kuriyama S, Tominaga K, Okuda H, Nakatani T, Yoshiji H, et al. Intravenous readministration of an adenoviral vector performed long after the initial administration failed to induce re-expression of the original transgene in rats. Int J Oncol. 2001; 18(3):575–80. [PubMed: 11179489]
41. Nong Z, Hoylaerts M, Van Pelt N, Collen D, Janssens S. Nitric oxide inhalation inhibits platelet aggregation and platelet-mediated pulmonary thrombosis in rats. Circ Res. 1997; 81(5):865–9. [PubMed: 9351461]
42. Roe ND, Ren J. Nitric oxide synthase uncoupling: a therapeutic target in cardiovascular diseases. Vascul Pharmacol. 2012; 57(5–6):168–72. [PubMed: 22361333]
43. Barbato JE, Zuckerbraun BS, Overhaus M, Raman KG, Tzeng E. Nitric oxide modulates vascular inflammation and intimal hyperplasia in insulin resistance and the metabolic syndrome. Am J Physiol Heart Circ Physiol. 2005; 289(1):H228–36. [PubMed: 15734883]
44. Shears LL 2nd, Kibbe MR, Murdock AD, Billiar TR, Lizonova A, Kovesdi I, et al. Efficient inhibition of intimal hyperplasia by adenovirus-mediated inducible nitric oxide synthase gene transfer to rats and pigs in vivo. J Am Coll Surg. 1998; 187(3):295–306. [PubMed: 9740187]
45. Finn AV, Joner M, Nakazawa G, Kolodgie F, Newell J, John MC, et al. Pathological correlates of late drug-eluting stent thrombosis: strut coverage as a marker of endothelialization. Circulation. 2007; 115(18):2435–41. [PubMed: 17438147]
46. Kibos A, Campeanu A, Tintoiu I. Pathophysiology of coronary artery in-stent restenosis. Acute Card Care. 2007; 9(2):111–9. [PubMed: 17573586]

47. Li H, Horke S, Forstermann U. Vascular oxidative stress, nitric oxide and atherosclerosis. Atherosclerosis. 2014; 237(1):208–19. [PubMed: 25244505]

48. Maillard L, Van Belle E, Tio FO, Rivard A, Kearney M, Branellec D, et al. Effect of percutaneous adenovirus-mediated Gax gene delivery to the arterial wall in double-injured atheromatous stented rabbit iliac arteries. Gene Ther. 2000; 7(16):1353–1361. [PubMed: 10981661]

49. Llano R, Winsor-Hines D, Patel DB, Seifert PS, Hamamdzic D, Wilson GJ, et al. Vascular responses to drug-eluting and bare metal stents in diabetic/hypercholesterolemic and nonatherosclerotic porcine coronary arteries. Circ Cardiovasc Interv. 2011; 4(5):438–46. [PubMed: 21972400]

50. Piedra J, Ontiveros M, Miravet S, Penalva C, Monfar M, Chillon M. Development of a rapid, robust, and universal picogreen-based method to titer adeno-associated vectors. Hum Gene Ther Methods. 2015; 26(1):35–42. [PubMed: 25640021]

51. Fishbein I, Welch T, Guerrero DT, Alferiev IS, Adamo RF, Chorny M, et al. Paraffin processing of stented arteries using a postfixation dissolution of metallic and polymeric stents. Cardiovasc Pathol. 2016; 25(6):483–488. [PubMed: 27616613]

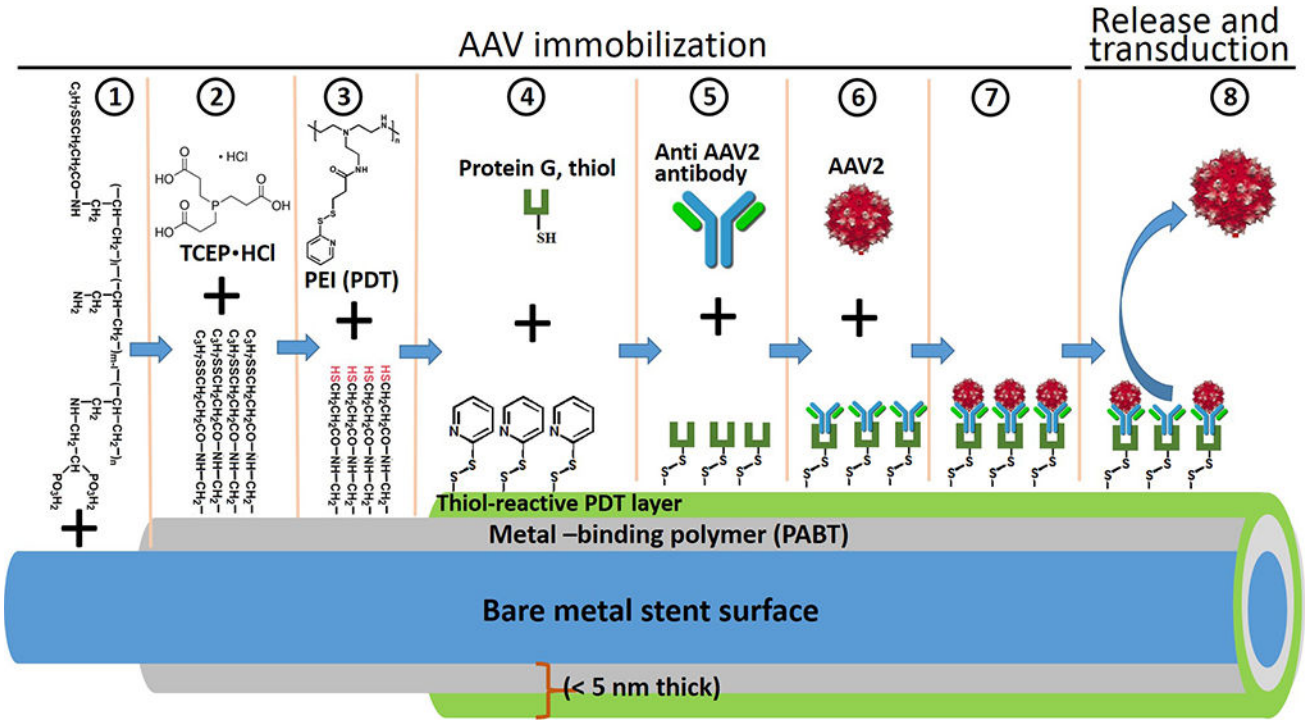

Figure 1. The principal scheme of gene vector immobilization

Reversible attachment of gene vectors to the bare metal surface of the stents was achieved by the sequential exposure of stents or model metal samples to 1) polyallylamine bisphosphonate with latent thiol groups (PABT, [7]); 2) tris-(2-carboxyethyl) phosphine (TCEP·HCL); 3) pyridyldithio-engrafted polyethyleneimine (PEI-PDT, [7]); 4) thiolated protein G; 5) vector-capturing antibody and 6) vector suspension resulting in 7) immobilization of vector particles on the metal substrate and 8) their subsequent release from the surface.

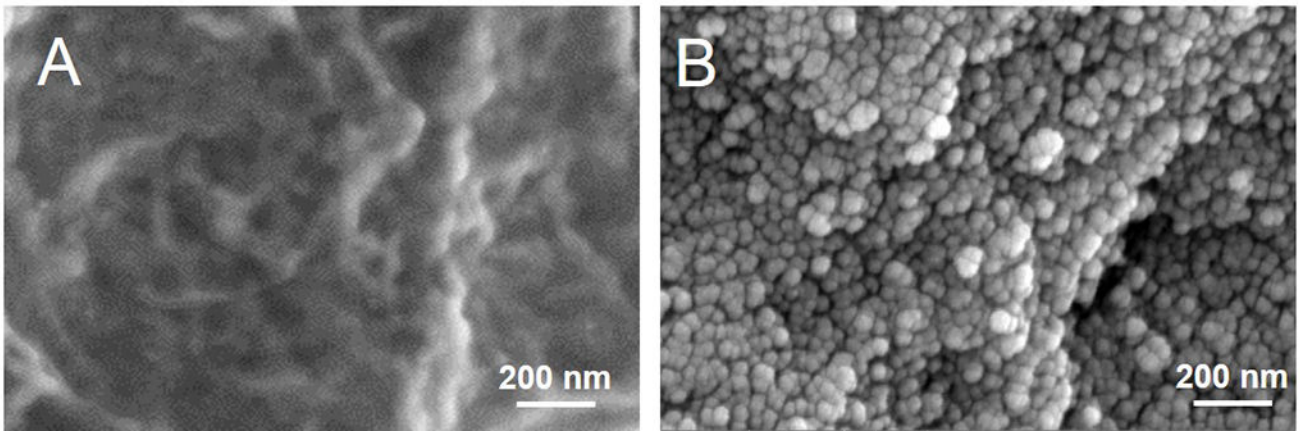

Figure 2. Scanning electron microscopy

Representative electron microscopy images of (A) bare metal stainless steel mesh disks and B) mesh samples formulated according to the PrG/A20 tethering protocol and incubated with AAV2 vector demonstrating surface coverage with viral capsids. Original magnification is 80,000x.

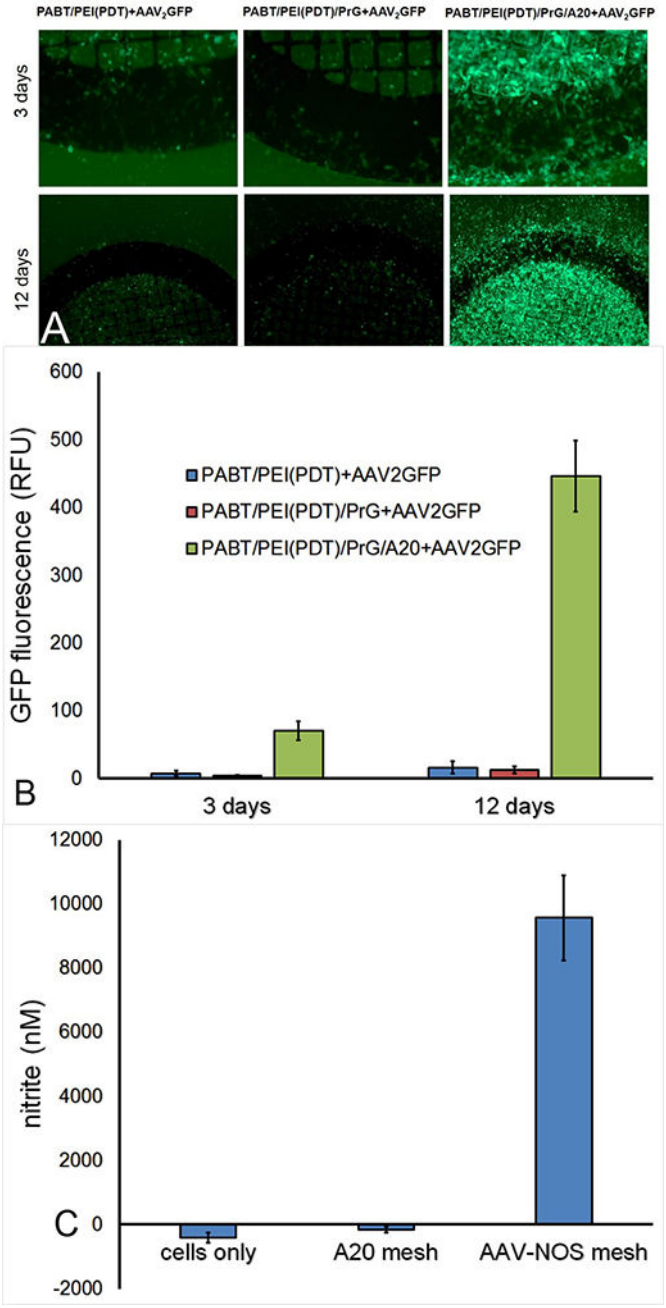

Figure 3. Cell transduction with mesh-immobilized AAV2 vectors

(A) Representative fluorescence microscopy images and (B) quantitative fluorimetric data of 3 and 12 day HEK293 cell cultures transduced with mesh disks configured with $AAV2_{eGFP}$ vector immobilized via PrG/A20 tether (A, right) or with similarly $AAV2_{eGFP}$-exposed meshes lacking either A20 antibody (A, middle) or both PrG and A20 antibody (A, left) components of the tether. Original magnifications are 200x (day 3) and 100x (day 12). Spectrophotometric data (C) demonstrating nitrite accumulation per Griess assay in media conditioned with HEK293 cells transduced with $AAV2_{iNOS}$ attached to the bare stainless steel mesh using the PrG/A20 tethering strategy (right). Nitrite levels in the media

conditioned with untreated HEK 293 cells (left) and HEK 293 treated with PrG/A20 meshes that were not exposed to $AAV2_{iNOS}$ (middle) were used as controls.

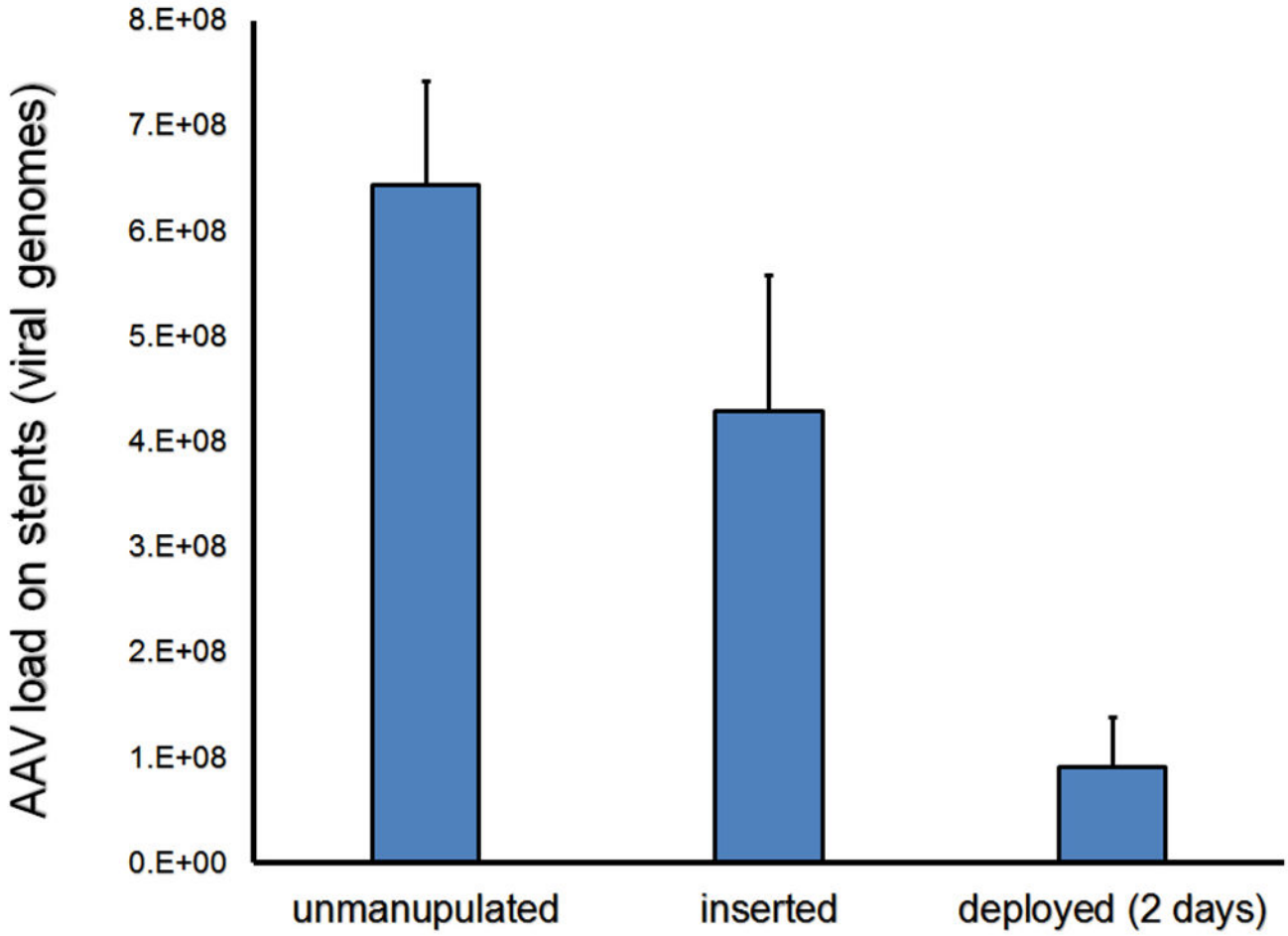

Figure 4. Modulation of AAV2 load during stent deployment and subsequent release *in vivo*

RT-PCR-based quantification of the number of surface-associated $AAV2_{eGFP}$ vector genomes in stent samples that were either 1) expanded *ex vivo* (n=4); 2) inserted into the common carotid artery in rats, removed undeployed, and then expanded *ex vivo* (n=4) or 3) deployed in the common carotid arteries and harvested 2 days after surgery (n=4).

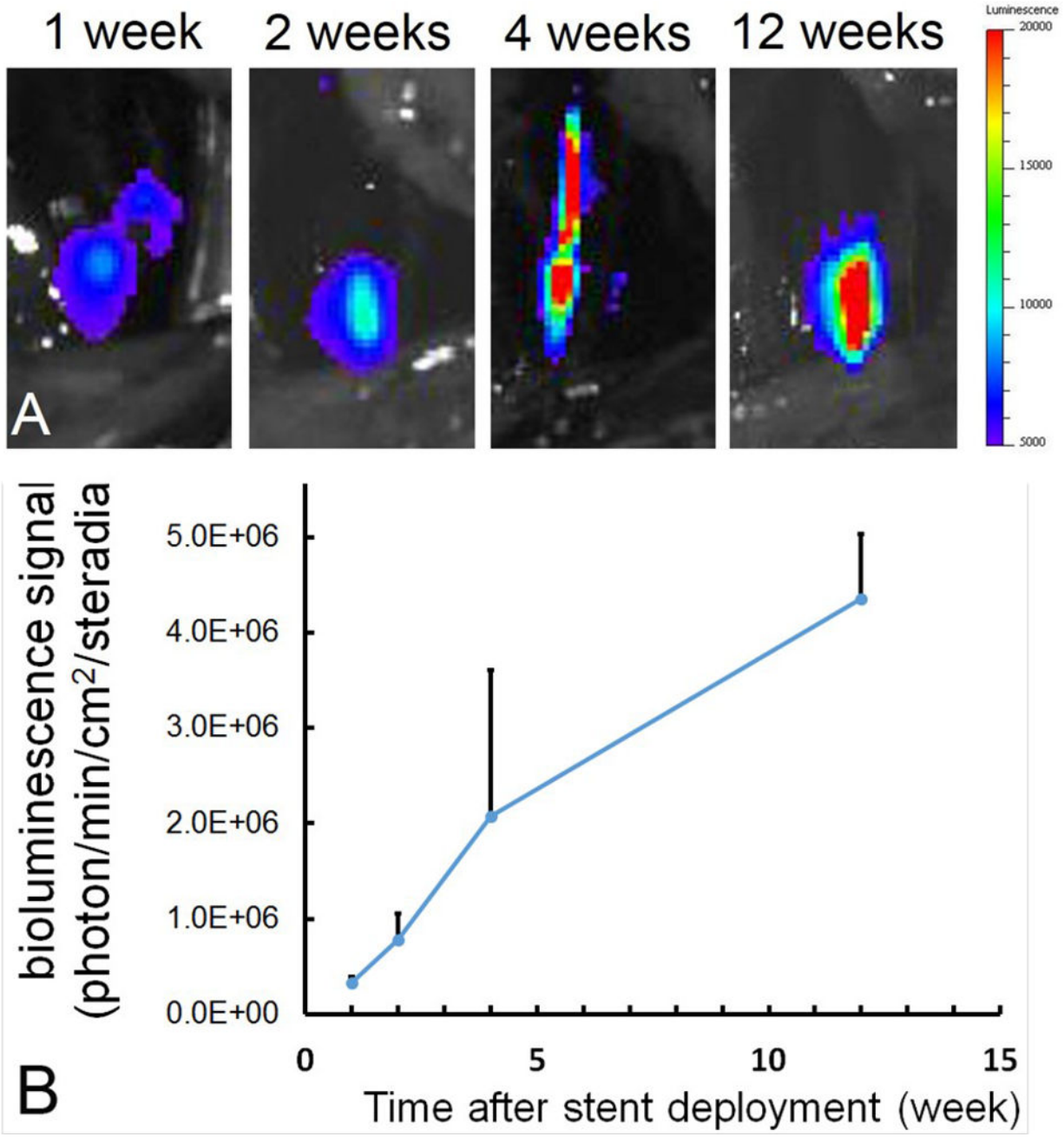

Figure 5. Longitudinal detection of arterial transduction following AAV2$_{Luc}$ stent deployment by bioluminescence imaging

Imaging series (A) showing typical dynamics of luminescence signal emitted from AAV2$_{Luc}$ stent-transduced rat common carotid arteries and (B) quantitative imaging data plotted as a function of time.

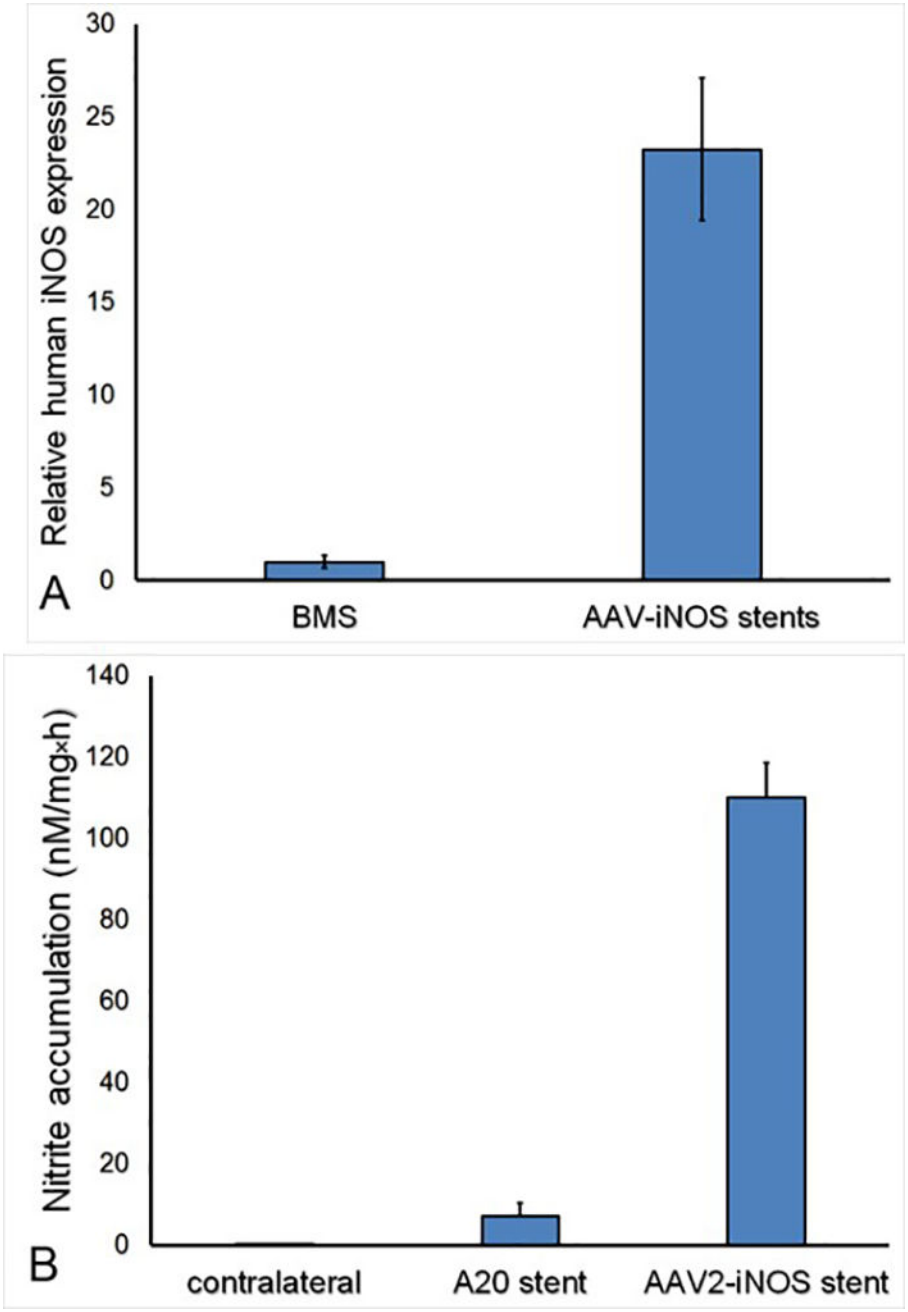

Figure 6. Functional transgene expression in the AAV2$_{iNOS}$ stent-treated rat arteries

(A) Fold increase of human iNOS expression in rat carotid arteries treated with AAV2$_{iNOS}$ gene delivery stents (n=4) vs bare metal stents (n=4) per RT-PCR (ΔΔCt calculation method). The expressed transgene is functionally active as evidenced by (B) nitrite accumulation in the media conditioned by carotid arteries (n=4) harvested 8 days after AAV2$_{iNOS}$ stent implantation in the rat carotid model and maintained in organ culture for 72 hours, compared to the similarly processed arteries treated with BMS (n=4) and non-stented contralateral right carotid arteries (n=4).

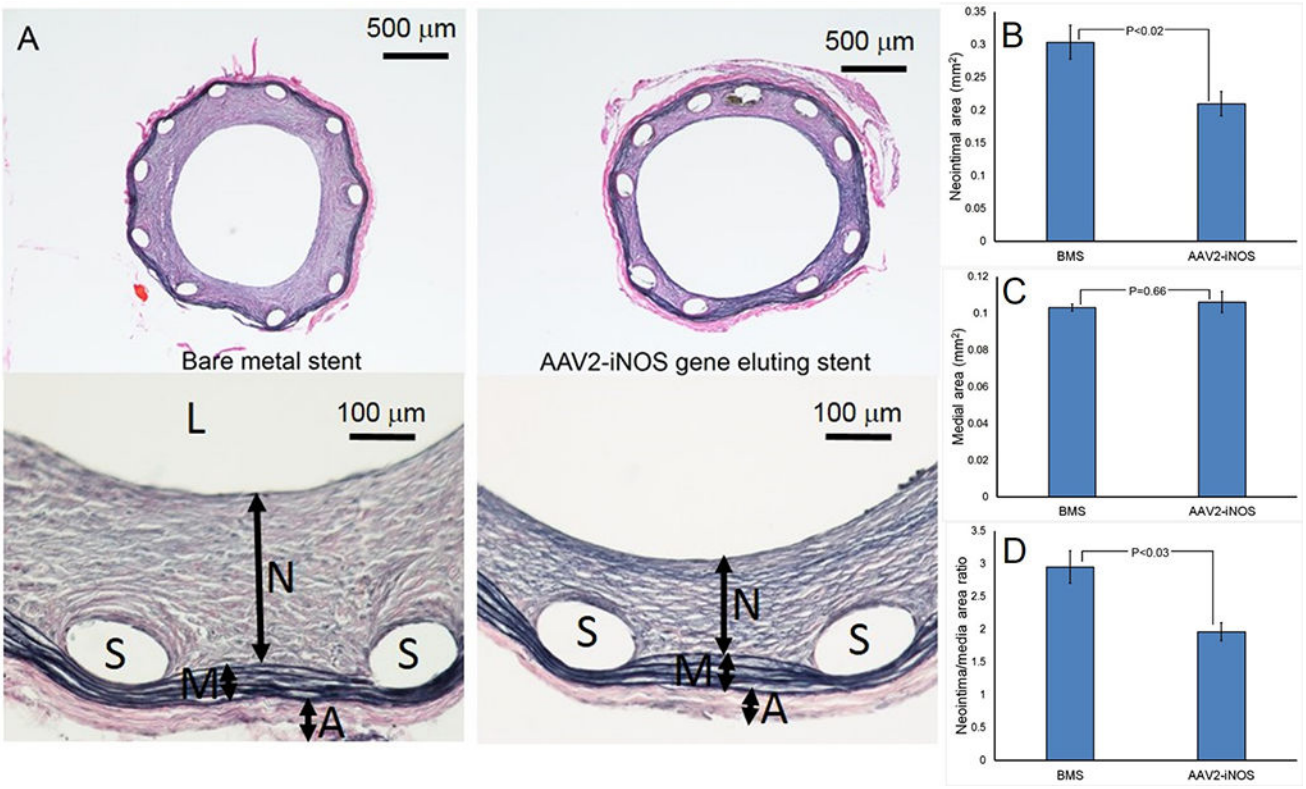

Figure 7. ISR inhibition by AAV2$_{iNOS}$ - eluting stents in the rat carotid model

Representative images of Verhoeff-van Gieson stained arterial sections (A) obtained from the BMS-treated (n=10) and AAV2$_{iNOS}$-treated (n=10) rat carotid arteries. (B) Morphometric analysis of in-stent restenosis in the BMS-treated and AAV2$_{iNOS}$ eluting stent-treated rat carotid arteries. L, N, M, A and S denote lumen, neointima, media, adventitia and spaces left by dissolved stent struts, respectively.

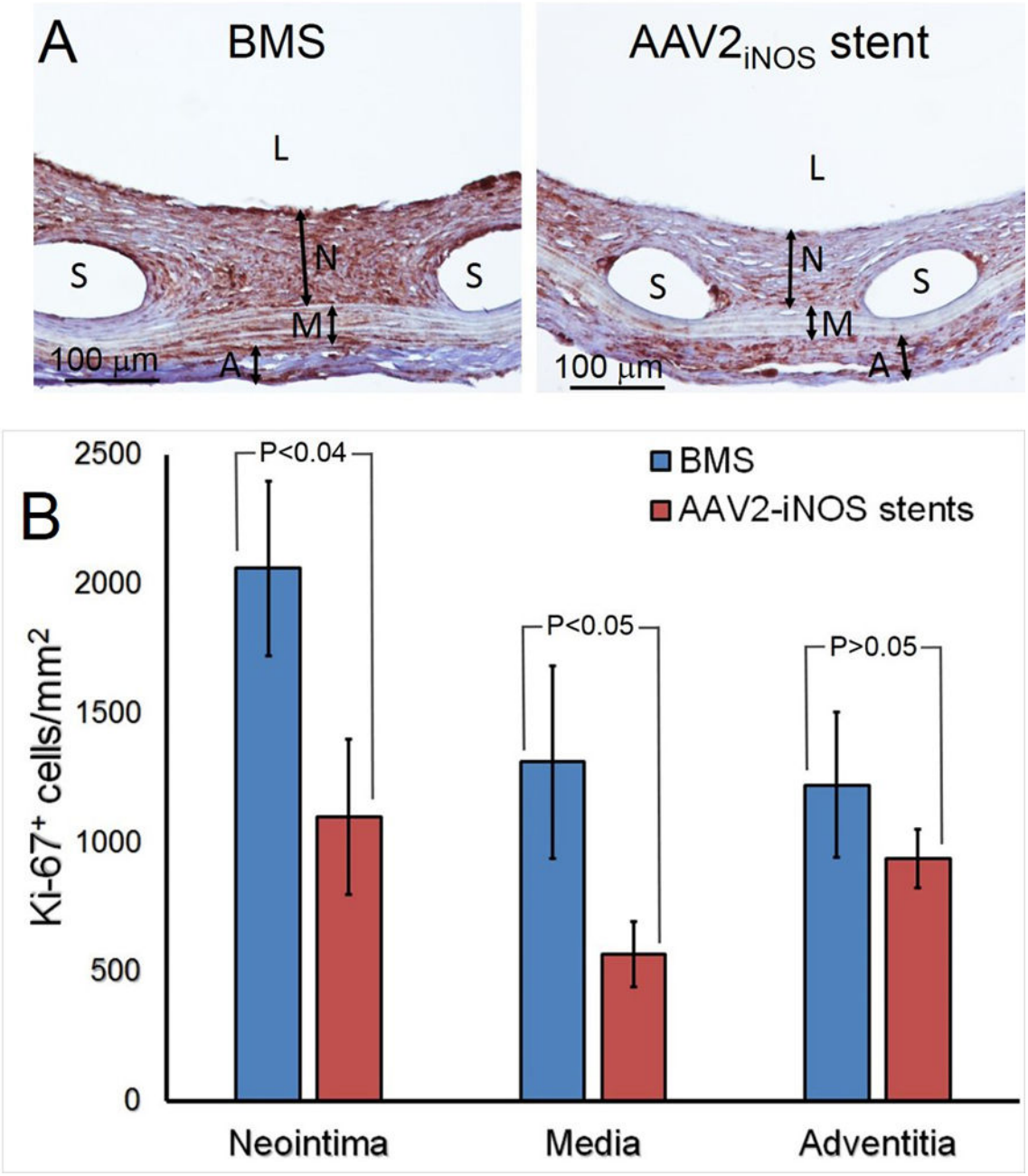

Figure 8. AAV2$_{iNOS}$ - eluting stents decrease proliferative activity in stented vasculature

(A) Representative immunohistochemical Ki-67 staining of BMS-treated (n=4; left) and AAV2$_{iNOS}$ GDS-treated (n=4; right) arteries.

(B) Ki-67 labeling density (number of positive cells/mm^2) in adventitia, media and neointima of stented arteries. L, N, M, A and S denote lumen, neointima, media, adventitia and spaces left by dissolved stent struts, respectively.